Synchronization with Molecular Signals on Spatial-Temporal Complex Networks

Lin Lin
University of Warwick, UK
Tongji University, Shanghai, China

Giannis Moutsinas
University of Warwick, UK

Cong Wu
Tongji University, Shanghai, China

Weisi Guo*
University of Warwick, UK

ABSTRACT

Molecular signals are fundamental to achieving synchronous functionality in both biological and bio-engineering systems. Synchronization on complex molecular signaling networks depend on both local diffusion-advection dynamics and the overall complex network topology. Here, we consider a spatial-temporal dynamic complex network with molecular signaling. Unlike current Kuramoto phase models that only consider scalar coupling between oscillator units, we introduce diffusion-advection lag that represents realistic molecular transportation processes. Our results across different networks and molecular dynamics show that the local connectivity status and dynamics dominate system-wide synchronization behaviour. We go on to create distributed control that can allow different networks to achieve similar overall synchronization profiles. We expect these findings to help the design of IoNT mesh networks and understanding of chrono-biological systems.

KEYWORDS

synchronization, complex networks, molecular communication

ACM Reference Format:
Lin Lin, Giannis Moutsinas, Cong Wu, and Weisi Guo. 2019. Synchronization with Molecular Signals on Spatial-Temporal Complex Networks. In *Proceedings of NanoCom '19: The 6th ACM International Conference on Nanoscale Computing and Communication (NanoCom '19).* ACM, New York, NY, USA, 6 pages. https://doi.org/

1 INTRODUCTION

Many essential biological activities inside living organisms have equilibrium periodicity, which are strongly coupled to external stimuli (e.g. sunrise-sunset, tidal and lunar rhythms for marine life) and affect both long-term hormone cycles to short-term gene oscillations. Stimuli that knock the clock out of equilibrium can cause undesirable side effects and illness [15]. For example, circadian clocks are biochemical oscillators that are synchronized with solar time with an equilibrium period of 23.8 hours [10]. One interesting aspect of circadian clocks is its resilience to external perturbations, whereby despite the abundance of different artificial light sources (e.g. indoor lighting and mobile phones screens after sunset), the temporal standard deviation is approximately 3 to 5 min each day. Singular oscillators cannot achieve this level of precision and it has been recently shown that highly coupled oscillators via a complex network can explain the collective enhancement of temporal synchronization precision [2]. Some research works study using inducer or inhibitory molecules to realize the network wide synchronization [1, 19].

1.1 Current Kuramoto Model

Current Kuramoto models are linear coupling models used to describe a variety of problems that can be described by networks of coupled dynamical systems [14]. The Kuramoto model tracks the phase rate of change $\dot{\phi}_i$ as a function of the inherent desirable or natural frequency ω_i in each unit and the coupling from connected neighbouring units j:

$$\dot{\phi}_i = \omega_i + \sum_{j,j\neq i} K_{ij} \sin(\phi_j - \phi_i) + L \sin(\Omega t - \phi_i) + \zeta(t), \quad (1)$$

where K_{ij} describes the scalar coupling complex network's connectivity matrix, and $\zeta(t)$ is a white Gaussian noise. The sinusoidal function $\sin(\phi_j - \phi_i)$ describes the positive or negative contribution to $\dot{\phi}_i$ depending on the sign of $(\phi_j - \phi_i)$. The optional perturbation signal $L \sin(\Omega t - \phi_i)$ describes a disturbance at frequency Ω.

A major drawback of many existing studies is that the coupling dynamics only focus on phase level coupling using scalar weights, but do not represent the spatial-temporal dynamics of molecular signals. As such, space (scale of the molecular signal propagation) and time (periodicity of the clock) are not factored into the Kuramoto framework. Whilst some work have considered diffusion dynamics [3, 22], they have not considered the joint effect of topology and dynamics in their analysis.

1.2 Contribution

In this paper, we investigate the synchronization process based on a model similar to the Kuramoto model, but take the diffusion-advection dynamics and graph topological properties into account. The rate of synchronization has two contexts. For chrono-biological

*Corresponding Author: weisi.guo@warwick.ac.uk. This work is funded by EC H2020 grant 792799.

NanoCom '19, September 25–27, 2019, Dublin, Ireland

ACM ISBN 978-1-4503-9999-9/18/06…$15.00
https://doi.org/

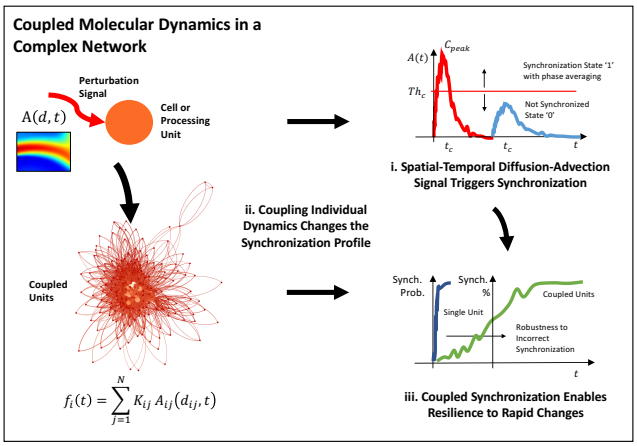

Figure 1: Negative perturbation causes synchronization to new signal in single and coupled systems: spatial-temporal diffusion-advection signal-to-noise ratio affect the decision for a unit to synchronize or not synchronize and coupling individual units changes the overall synchronization profile to be more resilient to external perturbations.

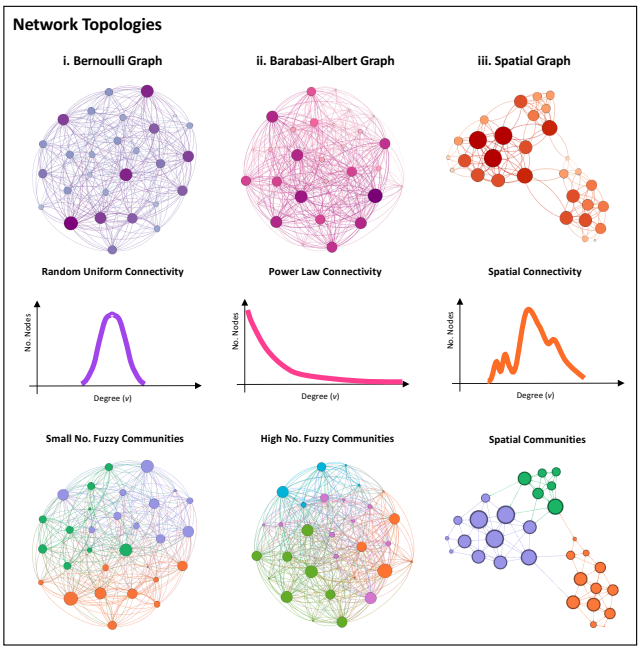

Figure 2: Different network topologies represent the real-world phenomenon of hubs and spatial embedding. Their degree distribution and community structure (modularity maximization) is shown.

systems, it gives us an understanding of how resilient the signaling network is against perturbation signals. For Internet-of-Nano-Things (IoNT) systems [4], this knowledge enables us to design effective mesh communication networks.

The academic insight lies in understanding synchronization rate's relationship with the complex network topology (e.g. graph degree distribution or spectral properties) and functional dynamics (e.g. diffusion-advection coupling between nodes). In order to consider the spatial-temporal aspects of molecular signaling, each coupling is a diffusion-advection function that is intimately related to the spatial graph structure. In this paper, we focus on the synchronization rate from non-equilibrium to equilibrium phase, whereby the rate is a proxy for the resilience of the system to external disturbances. Indeed, recent work by the authors in synchronization between a pair of molecular communication units have considered spatial temporal diffusion dynamics (e.g. using timing channels [16] with maximum likelihood estimation of offset [17]) and increasing robustness by using multiple receptors receiving the same synchronization signal to exploit path diversity [18].

The rest of the paper is organized as follows. In Section II, we define the system model. In Section III, we detail the synchronization methodology. In Section IV, we analyse the impact of graph structure and the dynamical molecular signals on the results, including looking at how molecular signal modulation control can give equivalent synchronization behaviour across different networks. Our results apply to both the circadian rhythm and the IoNT with molecular communication research communities.

2 SYSTEM MODEL

In our system, we assume a coupling network composed of N nodes. These nodes are identical in behaviour. Each node is assumed to be a processing unit (e.g. a cell or a nano-device) and each edge is a diffusion-advection molecular signaling pathway [12]. We assume the signaling edges do not interfere with each other (e.g. not a free-space diffusion environment where stochastic geometry analysis applies for cross-interference [9]). This is particularly valid in many realistic biological systems, whereby crowded cellular environment, constrained blood capillary vessels, and chemically specific pathways (e.g. no interference).

2.1 Coupling Network Structure

The K_{ij} connectivity matrix here is considered in the form of well-established random graph structures of different properties, see Fig. 2. The two properties of concern are: (i) **local degree distribution**, whereby the degree is the number of connections γ per node and this clearly affects the local rate of synchronization; and (ii) **regional community structure** [20], whereby highly connected communities of nodes are either all synchronized or all not synchronized.

Bernoulli Graph - We first consider a naive random graph, whereby nodes have a degree that follows a binomial distribution with probability of attachment as the control parameter. The communities are somewhat fuzzy due to the random preferential attachment of the graph generation, which means we expect synchronization to not be bottle-necked, see Fig. 3a. However, most real world networks are not uniformly and randomly connected in this way, due to the existence of heterogeneous structures (e.g. a heart or an internet router is more important) and preferential attachment (metric driven).

Barabasi-Albert Graph - As such, we then consider the Barabasi-Albert (BA) graph [6]. It has been shown that many natural and

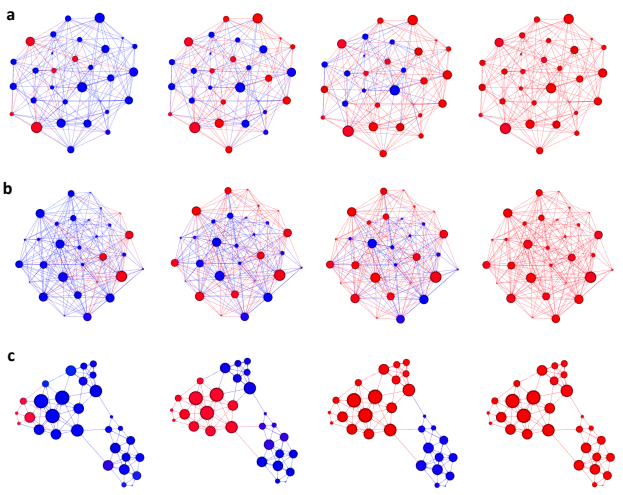

Figure 3: Synchronization with diffusion-advection dynamics at different representative time steps across: (a) Bernoulli uniform random graph, (b) Barabasi-Albert small-world random graph, and (c) Spatial graph with nested communities.

engineering systems (Internet) and some social networks can be well approximated by the scale-free network, where a few hubs dominate the network structure. The generates a scale-free networks using a preferential attachment probability (control parameter), whereby each node is connected to less than m nodes with probability: $p_i = \frac{\gamma_i}{\sum_j \gamma_j}$. This process gives nodes with a high number of connections a greater chance of being further connected. The degree distribution follows a power law, i.e. $P(\gamma) \sim \gamma^{-3}$. We expect the hubs to play a critical effect in synchronization rate, see Fig. 3b.

Spatial Graph - Many networks also exhibit spatial embedding [7], whereby small cliques of well connected nodes are nested in a larger network. This is because many interactions have high impedance, causing a strong bias towards well connected local coupling and weak global coupling. Spatial networks have a high clustering coefficient (control parameter) and are typically found in infrastructure networks, transport networks and neural networks. In spatial graphs, the meso-scale communities tend to be well defined (stable boundaries), which means we expect synchronization to be bottle-necked by community boundaries, see Fig. 3c. This is particularly relevant in diffusion-advection dynamics, whereby transportation of molecular signals is likely to be more reliable locally than across longer distances.

2.2 Diffusion-advection Molecular Signaling

Each edge in the coupling network is a molecular signaling pathway. The propagation is driven by mass diffusion with advection drift (low Peclet number), which is governed by [11]

$$A_{ij}(d,t) = \frac{1}{\sqrt{4\pi D t}} \exp\left[-\frac{(d_{ij} - vt)^2}{4Dt} \right], \tag{2}$$

where $A_{ij}(d,t)$ describes the coupling dynamic that is in the form of a 1-D diffusion-advection dynamic, with distance d_{ij}, flow velocity v, and diffusivity D. Here is the 1-D equation is chosen to represent molecular signals traveling in capillary blood vessels and active transport channels, where the length-scale dominates dynamics and the higher dimensions (e.g. width) doesn't dominate. It is worth noting that the dynamics can easily take on the 3-D form with or without an absorbing receiver [12]. We also do not consider factors such as the heart pump rate and shear stress from the wall in this paper. The receiver will use the information from the received or sensed molecules to perform the synchronization (see below).

3 SYNCHRONIZATION FRAMEWORK AND METHOD

In this section, the synchronization framework and method are presented based on the given network structure and a model similar to the Kuramoto model. The Kuramoto model focuses on the mathematical model of the phase interaction and synchronization, but lacks of the description of the synchronization process and does not mention the molecular diffusion-advection dynamics such as distance. More importantly, the spatial dynamics do not map back to the network structure. Here we take the diffusion-advection dynamics and graph structure into account.

As we focus on the synchronization rate as a function of diffusion-advection dynamics and define the propagation delay from node i to node j equal to the peak concentration time of the molecular signal at node j [23]. The peak concentration time can be calculated by taking the derivative of (2) with respect to t and setting it to zero. Then we have

$$T_c = \frac{d^2}{\sqrt{D^2 + v^2 d^2} + D}. \tag{3}$$

We now examine the synchronization framework and convergence properties.

3.1 Synchronization Between Two Nodes via Single Signaling Pathway

In first instance, an individual unit can receive an undesirable perturbation signal $A(d,t)$. To consider distance-dependent signal degradation in the synchronization process, we define a concentration threshold Th_c as a proxy for reliable detection [13]. If the arrived peak concentration of the molecular signals at the receiver is smaller than Th_c as (see Fig. 1): $C_{\mathrm{peak}} < \mathrm{Th}_c$, then the receiver will not use that signal for the synchronization operation. For synchronization, node j updates its own phase ϕ as:

$$\phi_j(t + \Delta t) = \frac{(\phi_i(t) + \phi_j(t))}{2} + \eta(t). \tag{4}$$

where $\eta(t)$ is additive noise from molecular arrival [21].

3.2 Synchronization Among All Nodes in the Complex Network

Different from centralized synchronization, where a reference node floods the network with a broadcast signal, the biological synchronization in living organisms is always realized in a distributed manner. That is to say, the nodes only interact with their neighbors. In the end, the whole network can converge to a certain phase to realize the synchronization. When the individual units are connected

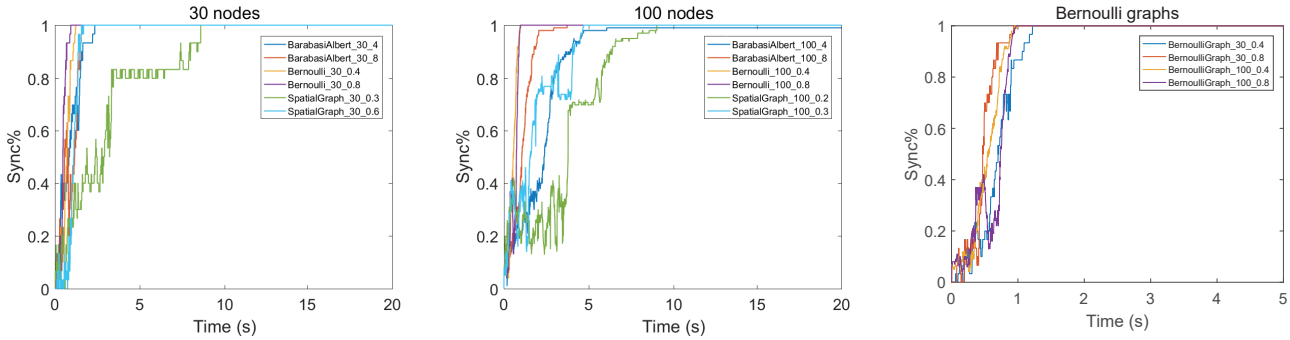

(a) Effect of graph type and connectivity. **(b) Effect of graph type and connectivity.** **(c) Effect of graph size and connectivity.**

Figure 4: Effect of global network topology on network synchronization rate.

together, the modified spatial-temporal synchronization system is given by a new function $g_i(t)$ which describes the synchronization signal strength:

$$g_i(t) = \sum_{j,j\neq i} K_{ij} A_{ij}(d,t). \tag{5}$$

It is assumed that the phase for node i at time t is denoted as $\phi_i(t)$. Then the updated phase, denoted as $\phi_i(t+\Delta t)$, can be expressed by

$$\phi_i(t+\Delta t) = f(\phi_i(t), g_i(t)). \tag{6}$$

where $f(\cdot)$ is the synchronization operation.

Proposition 1 *Synchronization leads to phase convergence.*

Proof. Assume that $P_{\max}$ and $P_{\min}$ are the maximum and minimum phase values among all the nodes in the complex network at the initial time. $P^n_{\max}$ and $P^n_{\min}$ are the maximum value and minimum value among the phase values of all the nodes after the nth round synchronization. For the $(n+1)$th round of synchronization, the maximum phase value would be averaged with some other phase values which are smaller than or equal to it. Then the result should be smaller than or equal to $P^n_{\max}$. If this result is the new maximum value after the $(n+1)$th round of synchronization, we can say $P^{n+1}_{\max} \leq P^n_{\max}$. If $P^{n+1}_{\max}$ is not from the averaging operation of $P^n_{\max}$, meaning that the averaging operation is performed from two values which is smaller than or equal to $P^n_{\max}$, then we can also obtain $P^{n+1}_{\max} \leq P^n_{\max}$. $P^{n+1}_{\max}$ is equal to $P^n_{\max}$ only when the two phase values for the averaging operation are equal to $P^n_{\max}$. From $P^0_{\max}$ to $P^n_{\max}$, until $P^{+\infty}_{\max}$, the maximum phase value is non-increasing over the whole synchronization time. Similarly, we have $P^{n+1}_{\min} \geq P^n_{\min}$, meaning that from $P^0_{\min}$ to $P^n_{\min}$, until $P^{+\infty}_{\min}$, the minimum phase value is non-decreasing over the whole synchronization time. As the averaging operation is conducted all the time, we can obtain that

$$\lim_{n->+\infty} P^n_{\max} = \lim_{n->+\infty} P^n_{\min} = P_c. \tag{7}$$

This demonstrates that the phase values of all the nodes in the complex network will converge to the certain value P_c finally. □

Next, to consider the quality of the synchronization, we would like to define how a node in the network is considered to be synchronized. If the phase of a node P(t) satisfies

$$|P(t) - P_c| < \mathrm{Th}_{\mathrm{sync}}, \tag{8}$$

where $\mathrm{Th}_{\mathrm{sync}}$ is a user defined threshold, then the node is considered to be synchronized. Otherwise it is considered that the synchronization fails. It should be noted that because the synchronization process, i.e., the phase averaging operation, is performed round-by-round, it is possible that a already synchronized node becomes not synchronized from a synchronized status after certain synchronization operation with its neighbor.

Finally, we would like to define the synchronization rate at time t as

$$\mathrm{SyncRate}(t, \mathrm{Th}_{\mathrm{sync}}) = \frac{\mathrm{Sum}(\{\phi_i(t) - P_c\} < \mathrm{Th}_{\mathrm{sync}})}{N}, \tag{9}$$

where Sum{} is a function which returns the number of elements in the array $\{\phi_i(t) - P_c\}$ which satisfies the inequality $\{\phi_i(t) - P_c\} < \mathrm{Th}_{\mathrm{sync}}$ at time t.

We will now in the results section consider the synchronization behaviour for a variety of network topology, signaling distance, and flow velocity values.

4 RESULTS

4.1 Simulation Setup

In a 2-dimensional simulation space, N nodes are deployed. The position of the nodes are randomly generated. The edges connecting those nodes are generated based on different network structures. In the Barabasi-Albert-N-m model, the m is the parameter of attachment. In the Bernoulli-N-p model, every edge has the same probability p. In the spatial network-N-r is drawn by getting N random nodes in the unit square and connecting the ones that are closer than some distance r.

For the synchronization process, every node begins with no natural frequency $\omega = 0$, a random uniformly distributed phase, which is the random non-equilibrium state. The nodes send synchronization signals via its diffusion-advection molecular signaling pathway once for each round. Once a node receives a synchronization signal, it takes average of its own phase and the phase of the

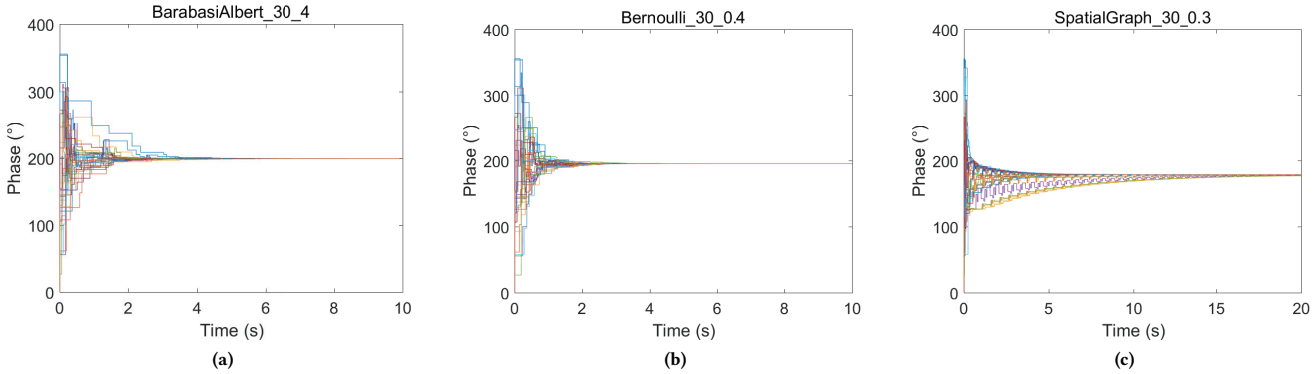

Figure 5: Phase convergence for different network structures.

Table 1: Simulation Parameters in SI Units

Parameters	Symbol	Values
distance ratio		0.7-1.3×10^{-5}
diffusivity	D	10^{-9} m^2/s
velocity	v	2 to 4 × 10^{-5} m/s
no. nodes	N	30 to 100
natural freq.	ω	0Hz
initial conditions	$\phi(0)$	random uniform phase

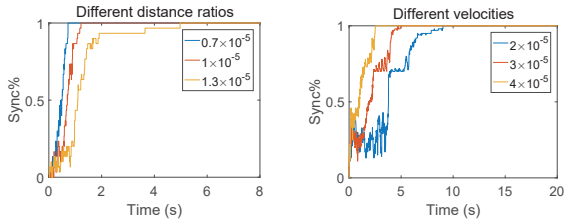

(a) Effect of distance between units. **(b) Effect of flow velocity.**

Figure 6: Effect of local diffusion-advection on overall networked synchronization rate.

received signal. The network performs the synchronization in a distributed manner until a homogeneous equilibrium is established. The simulation parameters are given in Table 1.

4.2 Graph Properties on Synchronization

Fig. 4 shows the effect of overall network topology on the network synchronization rate. We can see that the synchronization rate for the spatial graph with nested communities and poor connection between communities exhibit particularly high resilience to synchronization than other similar networks with same number of nodes and links. We can also see that the increase of the network size has a larger effect on the Barabasi-Albert (BA) graphs than on the Bernoulli graphs. The increase of the network size increases the convergence time for BA graphs, although the synchronization is performed in a distributed manner. It is not easy for BA graphs to converge rapidly. However from Fig. 4c, we can see the network size has little effect on the synchronization rate in a distributed manner for Bernoulli graph, a well connected graph. This is quite different from a centralized tree topology network.

4.3 Dynamic Properties on Synchronization

This leads nicely to local functional dynamics and their influence on global synchronization dynamics. In Fig. 6, we can see the effect of diffusion-advection dynamics on the synchronization rate. For greater distances between nodes, a 2-fold increase in distance will increase the synchronization time by 5-fold. Similarly, for increased flow velocity, a 2-fold increase in velocity leads to an also 5-fold increase in synchronization time. This can be easily understood that the increase of the distance ratio and the decrease of the velocities will cause the molecules to take a longer time to diffuse and arrive at the receiver for a certain edge according to (3).

One may also notice that the synchronization rate is not monotonically increasing. For example in Fig. 6b, it is seen that the synchronization rate fluctuates frequently. The reason is that the operation in (4) cannot guarantee that after every single synchronization behaviour between two nodes, the phase would be closer to the network convergence value. If the synchronization rate decreases, it means that a already synchronized nodes falls into the un-synchronized status due to the synchronization behaviour with another node. However, for a long run, the overall synchronization process will lead to a network convergence, as shown in Fig. 5. We can also note that the spatial graph converges more slowly than BA and Bernoulli graph. This is because of less connectivity among different clusters of nodes.

We also investigate the influence of the concentration threshold Th_c and the threshold $\mathrm{Th}_{\mathrm{sync}}$, which is used in the definition of "synchronization", on the synchronization rate. We can see in Fig. 7a that larger value of Th_c leads to slower synchronization of the network, because more signals are considered to be not large enough to be used for the synchronization. As in Fig. 7b, the increase of $\mathrm{Th}_{\mathrm{sync}}$ leads to a fast complex network synchronization, which can easily understood from (8).

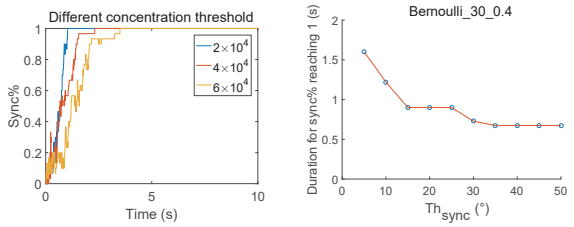

(a) (b)

Figure 7: Effect of concentration threshold and synchronization threshold.

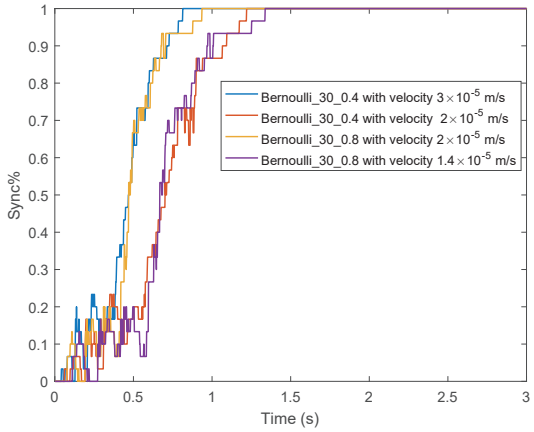

Figure 8: By adjusting weight parameters in the graph, we can achieve similar synchronization time profiles across different networks.

4.4 Network Equivalence using Distributed Control

So far in this paper, it is worth noticing that our graphs are randomly weighted graphs, where the adjacency matrix K_{ij} is unweighted and the diffusion-advection dynamics $A_{ij}(d,t)$ weights it. Interestingly, it has been recently shown that if we are able to configure the weights using maximum entropy or minimum KL divergence and within some constraint, we can achieve similar synchronization time profiles across different networks [5]. As it is often hard to change the network topology (e.g. predefined signal pathways), this opens up exciting possibilities to connect local functional optimisation (e.g. changing the diffusion-advection dynamics) and achieving optimal synchronization behaviour. Through distributed control of individual molecular signal concentration modulation, we can achieve a similar synchronization rate profile across different network topologies (see Fig. 8). Here, we use two Bernoulli networks with differing connectivity parameters of 0.4 and 0.8, resulting in different random networks. We tune the concentration arrival profile by tuning the average advection velocity to achieve similar synchronization profile between the two different networks.

5 CONCLUSION

Network synchronization via molecular signals is fundamental to chrono-biological functions and IoNT bio-engineering systems. We introduce spatial-temporal molecular propagation to the classical Kuramoto model, and analyse the impact of both topology and dynamics on synchronization rate. The simulation results show that the least constrained Bernoulli network synchronized faster, regardless of size. We also demonstrated that active control of the signal dynamics can achieve similar synchronization profiles amongst dramatically different complex network topologies, thus highlighting the importance of distributed control [8]. This will be investigated further in future research. The research has widespread implications in understanding chrono-biology as well as the design of future IoNT systems that require both synchronous action and resilience to both wanted and unwanted stimuli signals.

REFERENCES

[1] Sergi Abadal and Ian F Akyildiz. 2011. Bio-inspired synchronization for nanocommunication networks. In *Proc. IEEE GLOBECOM*. IEEE, 1–5.

[2] U. Abraham, A. Granada, P. Westermark, M. Heine, A. Kramer, and H. Herzel. 2010. Coupling governs entrainment range of circadian clocks. *Molecular Systems Biology* 6 (2010).

[3] J. Acebron, L. Bonilla, C. Perez Vicente, F. Ritort, and R. Spigler. 2005. The Kuramoto model: A simple paradigm for synchronization phenomena. *Reviews of Modern Physics* 77 (2005).

[4] I. Akyildiz, M. Pierobon, S. Balasubramaniam, and Y. Koucheryavy. 2015. The Internet of Bio-Nano things. *IEEE Commun. Mag.* 53, 3 (March 2015).

[5] L. Arola-Fernandez, A. Guilera, and A. Arenas. 2018. Synchronization invariance under network structural transformations. *Physical Review E* 97 (2018).

[6] A. Barabasi and R. Albert. 1999. Emergence of Scaling in Random Networks. *Science* 286 (1999).

[7] M. Barthelemy. 2011. Spatial networks. *Physics Reports* 499 (2011).

[8] Guanrong Chen. 2014. Pinning control and synchronization on complex dynamical networks. *International Journal of Control, Automation and Systems* 12, 2 (01 Apr 2014), 221–230.

[9] Y. Deng, A. Noel, W. Guo, A. Nallanathan, and M. Elkashlan. 2017. Analyzing Large-Scale Multiuser Molecular Communication via 3-D Stochastic Geometry. *IEEE Transactions on Molecular, Biological and Multi-Scale Communications* 3, 2 (June 2017), 118–133.

[10] R. Dallmann et al. 2012. The human circadian metabolome. *Proc. of the National Academy of Sciences (PNAS)* 109 (2012).

[11] Nariman Farsad, H Birkan Yilmaz, Andrew Eckford, Chan-Byoung Chae, and Weisi Guo. 2016. A comprehensive survey of recent advancements in molecular communication. *IEEE Commun. Surveys & Tut.* 18, 3 (2016), 1887–1919.

[12] W. Guo, T. Asyhari, N. Farsad, H. Yilmaz, A. Eckford, and C.B. Chae. 2016. Molecular communications: channel model and physical layer techniques. *IEEE Wireless Commun.* 23 (2016).

[13] W. Guo, S. Wang, A. Eckford, and J. Wu. 2013. Reliable communication envelopes of molecular diffusion channels. *Electronics Letters* 49, 19 (Sep. 2013), 1248–1249.

[14] Y. Hasegawa. 2018. Thermodynamics of collective enhancement of precision. *Physical Review E* 98 (2018).

[15] A. Kramer. 2015. Circadian rhythms. When the circadian clock becomes blind. *Science* 347 (2015).

[16] L. Lin, C. Yang, M. Ma, and S. Ma. 2015. Diffusion-based clock synch. for molecular comm. under inverse Gaussian distribution. *IEEE Sensors J.* 15 (2015).

[17] L. Lin, J. Zhang, M. Ma, and H. Yan. 2017. Time synchronization for molecular communication with drift. *IEEE Commun. Lett.* 21 (2017).

[18] Z. Luo, L. Lin, W. Guo, S. Wang, F. Liu, and H. Yan. 2018. One symbol blind synchronization in SIMO mMolecular Communication Systems. *IEEE Wireless Commun. Lett.* 7 (2018).

[19] Michael J Moore and Tadashi Nakano. 2013. Oscillation and synchronization of molecular machines by the diffusion of inhibitory molecules. *IEEE Trans. Nanotechol.* 12, 4 (May. 2013), 601–608.

[20] M. Newman. 2006. Modularity and community structure in networks. *Proc. of the National Academy of Sciences (PNAS)* 103 (2006).

[21] M. Pierobon and I. Akyildiz. 2011. Diffusion-Based Noise Analysis for Molecular Communication in Nanonetworks. *IEEE Trans. Signal Process.* 59 (2011).

[22] F. Rodrigues, T. Peron, P. Ji, and J. Kurths. 2016. The Kuramoto model in complex networks. *Physics Reports* 610 (2016).

[23] X. Wang, M. Higgins, and M. Leeson. 2015. Distance Estimation Schemes for Diffusion Based Molecular Comm. Systems. *IEEE Commun. Lett.* 19 (2015).